IN THE UNITED STATES PATENT AND TRADEMARK OFFICE

Applicant: Karine VALLE et al.

Application No.: 10/542,768   Group Art Unit: 1796

Filing or 371(c) Date: April 5, 2006   Examiner: Ling Siu Choi

Title: Organic-Inorganic Hybrid Material   Confirmation No.: 1613
Comprising a Mineral Mesoporous Phase and an
Organic Phase, a Membrane and Fuel Cell

DECLARATION

Commissioner for Patents
P.O. Box 1450
Alexandria, VA 22313-1450

Sir:

1.   I, Philippe BELLEVILLE, a citizen of France and residing at Tours, 25 rue Charles Gille, France, do hereby declare as follows:

2.   I am a senior scientist working at Commissariat à l'énergie atomique et aux énergies alternatives (CEA) R&D unit since March 1991, after having graduated from Pierre and Marie Curie University of Paris (Ph.D. in chemistry).

3.   Since 1991, I have been working in material chemistry, more precisely in smooth chemistry and hybrid organic-inorganic material preparation and development. I am an author of 40 scientific papers and an inventor on more than 20 patents. I have been a member of the Board of Directors of the International Sol-Gel Society (ISGS) since 2007 and am the recipient of the 2003 Ulrich Award for Excellence in Sol-Gel Technology. Therefore, I am fully conversant with the technical field to which the invention disclosed and claimed in U.S. Application No. 10/542,768 belongs.

4.   I have read and understand U.S. Application No. 10/542,768 (the "'768 Application").

5.   I have read and fully understand U.S. Patent No. 5,342,521 to Bardot et al. ("Bardot"); Okur H.I. et al., "Synthesis of Stable Mesostructured Coupled Semiconductor Thin Films: meso-CdS-TiO$_2$ and meso-CdSe-TiO$_2$" Langmuir 26(1):538-544 (2010) ("Okur"); Dai, Q. et al., "Effect of Templates on the Structure and Stability of Ti-TMS"

Chinese Chemical Letters 10(3):267-268 (1999) ("Dai"); and Yue, Y. et al., "Synthesis of Mesoporous TiO_2 with a Crystalline Framework" Chem. Commun. 2000:1755-1756 ("Yue"). Okur, Dai and Yue are provided in Appendix A.

6.   I have reviewed the Office Action of May 24, 2010, for the '768 Application.

7.   The specification of the '768 Application states, "Typically, mesoporous materials are amorphous or crystalline metal oxides in which the pores are generally distributed randomly with a very broad distribution in the size of the pores. Structured mesoporous materials, called 'mesostructured' materials, correspond, for their part, to structured pore networks which exhibit an organized spatial layout of mesopores." See, page 5, lines 8-15.

8.   Bardot discloses a reverse osmosis or nanofiltration membrane and its production process. Bardot does not disclose an organic-inorganic hybrid material comprising two phases, a first, mineral phase and a second, organic phase, in which the first, mineral phase comprises a structured mesoporous network with open porosity, and wherein the structured mesoporous network exhibits an organized structure with a repeating unit.

9.   One of ordinary skill in the art would understand that a structured mesoporous network would not result from performing the steps outlined in Example 1 of Bardot. See, col. 4, lines 42-51.

10.   Relevant publications suggest that the structured mesoporous TiO_2 was first synthesized in 1995.[1]

11.   As such, one of ordinary skill in the art would conclude that because Bardot

---

[1] Yue states, "[t]he synthesis of mesoporous silica with a high surface area and uniform cylindrical mesopores, which was designated M41S, was first demonstrated in 1992. Since then, the use of surfactants and amphiphilic block copolymers to organize mesoporous structures has been extended to the preparation of non-silica mesoporous metal oxides. Mesoporous ... TiO_2 ... [has] been synthesized over the past few years.", citing an article by Antonelli, D.M. et al., Angew. Chem., Int. Ed. Engl. 34:2013 (1995) ("Antonelli"). See, page 1755, first paragraph. Antonelli was published in 1995. Dai states, "[a]lthough recent efforts have suggested that it should be possible to synthesize mesoporous materials from transition metal oxide by molecular self-assembly of organic tempting agents and inorganic oxides, but there are few reports of this technique successfully generating such materials which could maintain a stable mesoporous structure upon removal of the organic micelles. Recently, Antonelli et al. reported that a hexagonally packed purely mesoporous TiO_2 material (Ti-TMS) was accomplished through a usual modified sol process." See, page 267, first paragraph. Okur states, "[a]fter the first synthesis of mesostructured titania in 1995, the field progressed very slowly until 2004.", citing Antonelli. See, page 538, first paragraph.

was filed before 1995, Bardot does not disclose a structured mesoporous TiO_2.

12.   The undersigned petitioner declares further that all statements made herein of his own knowledge are true and that all statements made on information and belief are believed to be true, and further that these statements were made with the knowledge that willful false statements and the like so made are punishable by fine or imprisonment, or both, under Section 1001 of Title 18 of the United States Code and that such willful false statements may jeopardize the validity of this application or any patent issuing thereon.

Date: October 5, 2010

_____

Philippe Belleville

Appendix A

Effect of Templates on the Structure and Stability of Ti-TMS

Qing DAI[1,2], Nong Yue HE[1], Xing Li WANG[2], Xun Wei SHEN[1], Yan GUO[1], Chun Wei YUAN[1]*

[1]National Laboratory of Molecular and Biomolecular Electronics,
[2]Department of Chemistry and Chemical Engineering, Southeast University, Nanjing 210096

Abstract: Pure Mesoporous TiO_2 molecular sieves (Ti-TMS) were synthesized with different templates for the first time and the templates can be successfully removed by refluxing the samples in the $EtOH/H_2O/KOH$ solution. The XRD pattern and TEM confirm that the uniformity and stability of Ti-TMS2 synthesized with dodecylamine as template is obviously inferior to that of Ti-TMS1 prepared with dodecylphosphate and hexadecylphosphate as templates. Furthermore, after the templates were removed, the mesostructure of Ti-TMS1 was preserved to a great degree than that of Ti-TMS2.

Keywords: TiO_2; mesoporous molecular sieves; template.

Mesoporous materials are of great interest to catalysis because of their large and uniform pore size (20~100Å), which allow stereo-hindered molecules facile diffusion to internal active sites. Although recent effects have suggested that it should be possible to synthesize mesoporous materials from transition metal oxide by molecular self-assembly of organic tempting agents and inorganic oxides[1], but there are few reports of this technique successfully generating such materials which could maintain a stable mesoporous structure upon removal of the organic micelles[2,3]. Recently, Antonelli *et al* reported that a hexagonally packed purely mesoporous TiO_2 material (Ti-TMS) was accomplished through a usual modified sol process. The strategy was just successful with tetradecyl-phosphate surfactants[4]. Herein we first report some studies with other surfactants.

In our experiments, two approaches to the synthesis of Ti-TMS have been adopted. One method involved a modified method described by Antonelli *et al*. We employed acetylacetone to slow down the condensation of the titanium alkoxide precursor, thus allowing the titanium to interact with dodecyl- and hexadecylphophate templates before the metal alkoxide formed an insoluble titanate. The templates was first removed at pH=9 in the $EtOH/H_2O$ solution. The second method we developed just relied on the formation of a discrete covalent bond between the titanium alkoxide and the dodecyl-amine prior to hydrolysis. All samples were characterized by low-angle XRD and TEM. The results clearly display the hexagonal array of the mesopores.

Figure 1 indicated that two samples showed typical XRD of Ti-TMS1. The d-spacing for the (100) reflection appears at about 35Å, the secondary (110), (200), (210)

reflections appear between of 4° and 7° 2θ. Our experiments showed that the length of the hydrocarbon tail of the alkylphosphate can be used to vary the pore size of Ti-TMS1 and the longer the hydrocarbon tail of the alkylphosphate are, the better the structure and uniformity are. There is a considerable increasing in the intensity and sharpness of the patterns for our samples after removal of hexadecylphosphate by reflux in $EtOH/H_2O$ mixture at pH=7 for 24h, as compared to the XRD patterns of the samples reported by Antonelli *et al*, in which the template was removed by calcination at 350°C for 4h. This suggested that there is loss of structure and reduction in crystalline domain size on calcination more than on reflux with solution. From **Figure 2**, we can conclude that Ti-TMS2 are synthesized successfully. After removal of the template with $EtOH/H_2O$ mixture at pH=7, the intensity and stability are increased. But compared **Figure 1** with **Figure 2**, we also found that the stablity and uniformity of the pure TiO_2 mesostructure with alkylamine surfactant is obviously not as good as the one with alkylphosphate surfactant.

Figure 1. XRD patterns of Ti-TMS1 prepared by: a) hexadecylphosphate after the template removal, b) hexadecylphosphate before the template removal, c) dodecylphosphate before the template removal
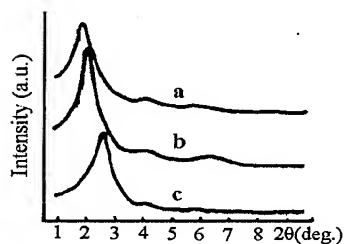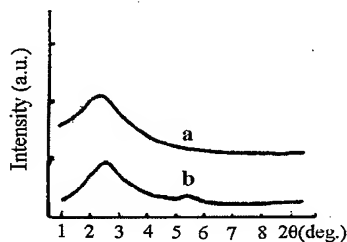
Figure 2. XRD patterns of Ti-TMS2 prepared by: a) dodecylamine after the template removal, b) dodecylamine before the template removal.

Acknowledgments

References

1. D. M. Antonelli, A. Nakahira, and J. Y. Ying, *Inorg. Chem.*, **1995**, *35*, 3126.
2. Q. Huo, D. I. Margolese, U. Cielsa *et al*, *Nature*, **1994**, *368*, 317.
3. U. Ciesla, D. Demuth, R. Leon *et al*, *J. Chem. Soc. Chem. Common.*, **1994**, 1387.
4. D. M. Antonelli, J. Y. Ying, *Angew. Chem. Int. Ed. Engl.* **1995**, *34*, 2014.

Received 3 June 1998

Synthesis of Stable Mesostructured Coupled Semiconductor Thin Films: meso-CdS-TiO$_2$ and meso-CdSe-TiO$_2$

Halil İ. Okur, Yurdanur Türker, and Ömer Dag*

Department of Chemistry, Bilkent University, 06800 Ankara, Turkey

Received June 24, 2009. Revised Manuscript Received July 7, 2009

Cd(II) ions can be incorporated into the channels of mesostructured titania films, using the evaporation-induced self-assembly (EISA) approach, up to a record high Cd/Ti mole ratio of 25%. The film samples were obtained by spin or dip coating from a mixture of 1-butanol, [Cd(H$_2$O)$_4$](NO$_3$)$_2$, HNO$_3$, and Ti(OC$_4$H$_9$)$_4$ and then aging the samples under 50% humidity at 30 °C (denoted as meso-xCd(II)-yTiO$_2$). The nitrate ions, from nitric acid and cadmium nitrate, play important roles in the assembly process by coordinating as bidentate and bridged ligands to Cd(II) and Ti(IV) sites, respectively, in the mesostructured titania films. The film samples can be reacted under a H$_2$S (or H$_2$Se) gas atmosphere to produce CdS (or CdSe) on the channel surface and/or pore walls. However, the presence of such a large number of nitrate ions in the film samples also yields an extensive amount of nitric acid upon H$_2$S (or H$_2$Se) reaction, where the nanoparticles are not stable (they undergo decomposition back to metal ion and H$_2$S or H$_2$Se gas). However, this problem can be overcome by further aging the samples at 130 °C for a few hours before H$_2$S (or H$_2$Se) reaction. This step removes about 90% of the nitrate ions, eliminates the nitric acid production step, and stabilizes the CdS nanoparticles on the surface and/or walls of the pores of the coupled semiconductor films, denoted as meso-xCdS-yTiO$_2$. However, the H$_2$Se reaction, additionally, needs to be carried at lower H$_2$Se pressures in an N$_2$ atmosphere to produce stable CdSe nanoparticles on the surface and/or walls of the pores of the films, denoted as meso-xCdSe-yTiO$_2$. Otherwise, an excessive number of Se$_8$ particles form in the film samples.

Introduction

After the first synthesis of mesostructured titania in 1995,[1] the field progressed very slowly until 2004.[2-8] The major problem is the difficulty in controlling the hydrolysis and condensation of titania precursors.[3] However, the use of 1-butanol as a solvent under acidic conditions and P123 as a template resolved some of those difficulties[9-11] to produce well-ordered transparent titania films.[9-15] However, the method requires large quantities of hydrochloric acid, which causes the contamination of the mesostructured titania films with Cl⁻ ions as charge-balancing counteranions on the titania surface. Notice also that the evaporation-induced self-assembly (EISA) process leaves the inorganic ingredients in the film samples as impurities. It is necessary to remove these ions from the mesostructured titania for many applications. The Cl⁻ ions can be removed from the mesostructured titania films by heating the samples to over 200 °C.[9] At this temperature, the surfactant molecules also burn and cause further contamination in the samples.[9] Therefore, it may be necessary to use an acid source that either does not contaminate the film samples (this is very unlikely) or decomposes at lower temperatures. Note also that the P123 molecules start decomposing from propoxides as low as 150 °C and calcination is complete at around 300 °C.[9] The nitrate ion is a good candidate because (i) it has a low decomposition (or removal) temperature, (ii) it plays a useful role in the self-assembly of organic (surfactant) and inorganic ingredients, and (iii) the transition-metal nitrate salts have higher solubility in the reaction media and in the as-synthesized mesostructured materials.

Large quantities of the metal nitrate salts can be dissolved in the hydrophilic domains of a salt-pluronic lyotropic liquid-crystalline mesophase[16] and in solid media such as in the mesostructured silica film.[17] However, the transition-metal chloride salts have limited solubility under typical mesostructured titania synthesis conditions. Therefore, it is important to change the salt and acid sources to metal nitrates and nitric acid, respectively. The nitrate ions play important roles in the self-assembly process by coordinating to the metal ion as a mono- or bidentate ligand via exchange with the coordinated water molecules.[18] Coordination of the nitrate ion to the metal centers reduces the charge and ion densities of the self-assembling media, which enhances the solubility of the nitrate salts.[16,18] The ligand-exchange reaction can be monitored best using FTIR and Raman techniques.[16,18]

*Corresponding author. E-mail: dag@fen.bilkent.edu.tr. Fax: 90-312-266-4068. Tel: 90-312-266-3918.

(1) Antonelli, D. M.; Ying, J. Y. *Angew. Chem., Int. Ed. Engl.* **1995**, *34*, 2014.

(2) Yang, P.; Zhao, D.; Margoles, D. I.; Chmelka, B. F.; Stucky, G. D. *Nature* **1998**, *396*, 152.

(3) Khushalani, D.; Dag, Ö.; Kuperman, A.; Ozin, G. A. *J. Mater. Chem.* **1999**, *9*, 1491.

(4) Yang, P.; Zhao, D.; Margoles, D. I.; Chmelka, B. F.; Stucky, G. D. *Chem. Mater.* **1999**, *11*, 2813.

(5) Soler-Illia, G. J. A. A.; Babonneau, F.; Sanchez, C.; Albouy, P. A.; Brunet-Bruneau, A.; Balkenende, A. R. *Adv. Mater.* **2001**, *13*, 1085.

(6) Soler-Illia, G. J. A. A.; Louis, A.; Sanchez, C. *Chem. Mater.* **2002**, *14*, 750.

(7) Crepaldi, E. L.; Soler-Illia, G. J. A. A.; Crosso, D.; Cagnol, F.; Ribot, F.; Sanchez, C. *J. Am. Chem. Soc.* **2003**, *125*, 9770.

(8) Dag, Ö.; Soten, I.; Çelik, Ö.; Polarz, S.; Coombs, N.; Ozin, G. A. *Adv. Funct. Mater.* **2003**, *13*, 30.

(9) Haseloh, S.; Choi, S. Y.; Mamak, M.; Coombs, N.; Petrov, S.; Chopra, N.; Ozin, G. A. *Chem. Commun.* **2004**, 1460.

(10) Choi, S. Y.; Mamak, M.; Coombs, N.; Chopra, N.; Ozin, G. A. *Adv. Funct. Mater.* **2004**, *14*, 335.

(11) Luo, H. M.; Wang, C.; Yan, Y. S. *Chem. Mater.* **2003**, *15*, 3841.

(12) Choi, S. Y.; Mamak, M.; Speakman, S.; Chopra, N.; Ozin, G. A. *Small* **2005**, *1*, 226.

(13) Choi, S. Y.; Lee, B.; Carew, D. B.; Mamak, M.; Peiris, F. C.; Speakman, S.; Chopra, N.; Ozin, G. A. *Adv. Funct. Mater.* **2006**, *16*, 1731.

(14) Wang, K. X.; Morris, M. A.; Holmes, J. D. *Chem. Mater.* **2005**, *17*, 1269.

(15) Liu, K. S.; Fu, H. G.; Shi, K. Y.; Xiao, F. S.; Jiang, L. Q.; Xin, B. F. *J. Phys. Chem. B* **2005**, *109*, 18719.

(16) Demirörs, A. F.; Eser, B. E.; Dag, Ö. *Langmuir* **2005**, *21*, 4156.

(17) Tura, C.; Coombs, N.; Dag, Ö. *Chem. Mater.* **2005**, *17*, 573.

(18) Dag, Ö.; Samarskaya, O.; Tura, A.; Günay, A.; Celik, Ö. *Langmuir* **2003**, *19*, 3671.

The doubly degenerate asymmetric stretching mode of the free nitrate ion, which is observed at around 1360 cm^{-1}, splits into two modes, observed in the 1280−1600 cm^{-1} region. The splitting energy between these two modes is 120−160 cm^{-1} in the monodentate, 160−210 cm^{-1} in the bidentate, and above 210 cm^{-1} in the bridged coordinated nitrate ions.[19] The symmetric stretching mode, which is Raman-active, is shifted from 1050 cm^{-1} to the 1010−1030 cm^{-1} range, which also becomes IR-active upon coordination.

The synthesis of stable CdS and CdSe nanoparticles on the channel surface or pore walls of mesostructured/mesoporous titania and CdSe-TiO$_2$ nanocomposites is important for many applications in fields such as efficient solar energy conversion and photocatalysis (the CdS and CdSe nanoparticles can function as an efficient sensitizers for the large band gap semiconductor TiO$_2$),[20−24] but so far, to the best of our knowledge, there are only a limited number of publications on the mesostructured CdS-TiO$_2$ and CdSe-TiO$_2$ materials.[25,26] In one of these publications, by Stucky and his group, the Cd(II) ions were incorporated into the mesostructured titania films using cadmium chloride salt (CdCl$_2$) during the synthesis step.[25] Although the Cl$^-$ ions enhance the micellization of the surfactants in the solution phase, the solubility of the chloride salt of the transition metals is limited when compared to the nitrate salts in the liquid-crystalline mesophases, which form in the early stages of the synthesis of the mesostructured film materials.[9] Therefore, the maximum amount of Cd(II) ion that can be incorporated using this approach is around 10 mol %.[25] The other group incorporated the presynthesized 4.2 nm CdSe nanoparticles with very low density, only 3 mol % (Cd/Ti), into the pores using a rapid immobilization method.[26] The metal sulfide or metal selenide nanoparticles can also be produced by first impregnating the metal ions into the pores and then reacting them with H$_2$S or H$_2$Se. However, this process also yields an extensive amount of acid that decomposes the nanoparticles. Note also that both impregnation (ions) and/or immobilization (nanoparticles) strategies yield nonuniform particle distributions in the channels. However, the transition-metal nitrate salts can be dissolved at relatively higher concentrations in the hydrophilic domains of the liquid-crystalline phase and remain solvated in the mesostructured film samples after the film becomes a rigid solid.[17] This is important in order to process a larger number of metal ions into the mesostructures to produce other metals, metal oxides, metal sulfides, and metal selenides on the pore walls of mesoporous materials.

In this contribution, we have investigated the role of nitrate ions in the assembly of Cd(II), Ti(IV), P123, 1-butanol, and acid mixtures and also in the stability of CdS and CdSe nanoparticles on the channel surface and/or pore walls of mesostructured titania thin films. The investigation has been carried out using X-ray diffraction (XRD), energy dispersive X-ray spectroscopy (EDS), transmission electron microscopy (TEM), UV−vis spectroscopy, and in particular, the role of the nitrate

has been investigated using the Fourier transform infrared (FTIR) spectroscopy technique.

Experimental Part

Preparation of Cd(II)-Modified Mesostructured Titania Films. Three sets of 0.0, 0.069, 0.173, 0.345, 0.449, and 0.518 g of [Cd(H$_2$O)$_4$](NO$_3$)$_2$ salt were dissolved in 6.0 g of 1-butanol in 20 mL vials. P123 (0.65 g) was added to each solution, and the solutions were stirred until all of the P123 completely dissolved. Upon addition of 1.0 g of concentrated HNO$_3$ to each vial, the mixtures were cooled in an ice bath for 1.5 min, and then 1.524, 2.286, and 3.048 g of Ti(OC$_4$H$_9$)$_4$ (Ti(IV)) was added to each of the above sets, set1, set2, and set3, respectively. Finally, the solutions were kept for 6 h with constant stirring in closed, sealed vials. In each set, the Ti(IV)/P123 mol ratios were kept at 40 (set1), 60 (set2), and 80 (set3), and the Cd(II)/P123 mol ratios were varied between 0 and 15 to prepare 18 samples with different compositions.

The film samples were prepared either by spin coating 1 mL of each of the above solutions onto a substrate at 500 rpm for 5 s and 1500 rpm for 20 s or dip coating a glass slides using a pulling speed of 0.4 mm/s. In total, 18 film samples were prepared for each H$_2$S and H$_2$Se reaction. The substrates were quartz or microscopy slides for the XRD and UV−vis measurements and silicon wafer for the SEM, EDS, Raman, and FTIR measurements. The film samples were further aged, immediately after preparation, first at 30 °C in a 50% humidity oven (Climacell 111) for 12 h and then at 130 °C in a regular oven for another 4 h. Then the samples were labeled as meso-xCd(II)-yTiO$_2$, where x and y are the initial Cd(II)/P123 and Ti(IV)/P123 mol ratios.

Preparation of CdS and CdSe Nanoparticles in Mesostructured Titania. Each film sample was exposed and kept under 200 Torr of H$_2$S for 5 min three times or under atmospheric pressure of 5−20% H$_2$Se in N$_2$ for 1 min in separate evacuated vacuum chambers. Upon completion of the reactions, the reaction cell was first evacuated into a trap with Cu(II)-loaded mesoporous silica to deposit unreacted H$_2$S or H$_2$Se as CuS or CuSe, respectively, for 2 min. The reaction chambers were then evacuated by pumping, using a rotary pump, for 5 min before removing the samples from the reaction chambers. The samples were labeled as meso-xCdS(or Se)-yTiO$_2$, where x and y are the initial Cd(II)/P123 and Ti(IV)/P123 mol ratios.

Instrumentation

The X-ray diffraction (XRD) patterns were recorded on a Rigaku Miniflex diffractometer using a Cu Kα source operating at 30 kV/15 mA (generating 1.5405 Å X-rays) and a Scintillator NaI(Tl) detector with a Be window. All of the XRD measurements were recorded using thin film samples on microscope slides. The FTIR spectra were recorded using a Bruker Tensor 27 FTIR spectrometer. A high-sensitivity DLATGS detector with a resolution of 4 cm^{-1} was used, and the spectra were collected from 128 scans. The FTIR spectra were recorded as thin films on a Si(100) wafer. The micro-Raman spectra were recorded on a LabRam confocal Raman microscope with a 300 mm focal length. The spectrometer is equipped with a Ventus LP 532 50 mW, diode-pumped, solid-state laser operated at 20 mW with a polarization ratio of 100:1 and a wavelength of a 532.1 nm and a 1024 element × 256 element CCD camera. The collected signal was transmitted via a fiber optic cable into a spectrometer with a 600 groove/mm grating. The Raman spectra were collected by manually placing the probe tip near the desired point of the sample on a silicon wafer. The UV−visible absorption spectra were recorded using a Varian Cary 5 double-beam spectrophotometer with a speed of 200 nm/min and a resolution of 2 nm over a wavelength range from 800 to 200 nm in transmittance mode.

(19) Nakamoto, K. *Infrared and Raman Spectra of Inorganic and Coordination Compounds*, Part A and B, 5th ed.; John Wiley & Sons: New York, 1997.

(20) Hester, R. E.; Scaife, C. W. *J. Chem. Phys.* 1967, *47*, 5253.

(21) Graetzal, M. *Nature* 2001, *414*, 338.

(22) Robel, I.; Subramanian, V.; Kuno, M.; Kamat, P. V. *J. Am. Chem. Soc.* 2006, *128*, 2385.

(23) Kim, J. Y.; Choi, S. B.; Noh, J. H.; Yoon, S. H.; Lee, S.; Noh, T. H.; Frank, A. J.; Hong, K. S. *Langmuir* 2009, *25*, 5348.

(24) Tvrdy, K.; Kamat, P. V. *J. Phys. Chem. A* 2009, *113*, 3765.

(25) Bartl, M. H.; Puls, S. P.; Tang, J.; Lichtenegger, H. C.; Stucky, G. D. *Angew. Chem., Int. Ed. Engl.* 2004, *43*, 3037.

(26) Shen, Y.; Bao, J.; Dai, N.; Wu, J.; Gu, F.; Tao, J. C.; Zhang, J. C. *Appl. Surf. Sci.* 2009, *255*, 3908.

Figure 1. Photographs of the transparent mesostructured film samples.

The UV regions were collected using film samples coated on quartz slides. The SEM images and the EDS data were obtained using a Zeiss EVO-40 SEM operating at 15 kV and a Bruker AXS XFlash detector 4010 attached to the same microscope using the same samples. The samples were prepared on silicon wafers that were attached to aluminum sample holders using conductive carbon adhesive tabs. The TEM images were collected using an FEI Tecnai G2 F30, operated at 200 kV. The film samples, first calcined at 250, 300, and 350 °C and then collected from the substrate, were finely ground in a morter and then dispersed into ethanol. A drop of the above dispersed ethanol solution was dried on a TEM grid for the TEM measurement.

Results and Discussion

A homogeneous, aged 1-butanol solution of Cd(II), Ti(IV), HNO_3, and P123 can be spin or dip coated onto various substrates, following an aging step, first under 50% humidity for 12 h at 30 °C and then at 130 °C for 4 h to produce well-ordered, transparent mesostructured titania films. The nitric acid and P123 content of the above solutions was kept the same in all 18 samples, which have been separately used for the H_2S and H_2Se reactions. The nitric acid concentration was optimized to determine the minimum amount of nitric acid necessary to prepare well-diffracting samples. The Ti(IV)/P123 mol ratios were kept at 40, 60, and 80 by changing the Cd(II)/P123 mol ratios from 0 to 15 to prepare the 18 film samples. The aging steps are critical to obtaining well-ordered film samples. No decomposition of the surfactant molecules is observed at 130 °C. The treatment of the film samples with a 200 Torr H_2S and 700 Torr 20% H_2Se/N_2 mixture, in a vacuum chamber, ensures the synthesis of stable CdS and CdSe nanoparticles, respectively, on the channel surface and pore walls of the transparent mesostructured titania films (Figure 1).

The film samples were further analyzed using TEM, XRD, EDS, UV−vis absorption, FTIR, and Raman techniques at each stage of the preparation to characterize the films structurally and to resolve the stability problems of the CdS and CdSe nanoparticles in the film samples. Note that the CdS or CdSe nanoparticles that are synthesized using fresh film samples, without the 130 °C aging step, decompose back to Cd(II) and H_2S or H_2Se, respectively. The CdS/TiO$_2$ and CdSe/TiO$_2$ w/w percentages in the stable, well-ordered mesostructured film samples can be increased up to 37 and 44% (equivalent to 25 mol %), respectively, using this approach. These are record high concentrations for both CdS
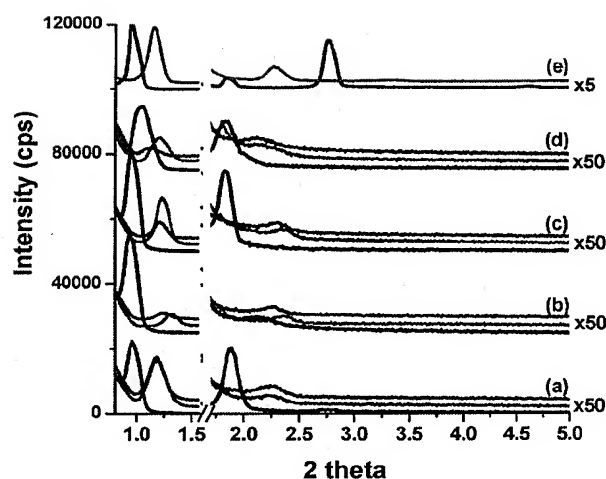

Figure 2. XRD patterns of a series of samples, prepared using a Ti/P123 mol ratio of 60 and Cd/P123 ratios of (a) 2, (b) 5, (c) 10, (d) 13, and (e) 0. The bottom samples (black) are as prepared, the middle samples (red) are after aging at 130 °C for 4 h, and the top samples (blue) are after H_2S reaction on each set. The two patterns in (e) are obtained from the Cd(II) free samples; the bottom is the fresh (black) and the top (red) is the aged (at 130 °C for 4 h) sample.

and CdSe using a one-pot synthesis approach. Recall that the highest CdS/TiO$_2$ quantity was only 10% in the literature.[25]

Figure 2 shows a series of XRD patterns of oriented meso-*x*Cd(II)-60TiO$_2$ (where *x* is 0, 2, 5, 10, and 13) films of as-prepared (fresh), aged (at 130 °C for 4 h), and after-H_2S-treatment samples. The structure remained at each stage in the above processes with some alteration in the unit cell and structural order. Each diffraction line gradually shifts to a higher angle; typically the small-angle line at 0.95° (92.9 Å *d* spacing) shifts to 1.22° (72.4 Å *d* spacing), 2θ upon aging, and shifts slightly to a lower angle or remains the same after H_2S (or H_2Se) treatment. This behavior indicates that the structure contracts as a result of further condensation of the titania walls and likely the formation of some Cd(OH)$_2$ and/or CdO species and then expands as a result of the formation of CdS (or CdSe) nanoparticles in the walls. The integrity of the film samples remains unaltered after all of the treatments. The TEM images show well-ordered channels oriented parallel to the film surface with curling channel patterns
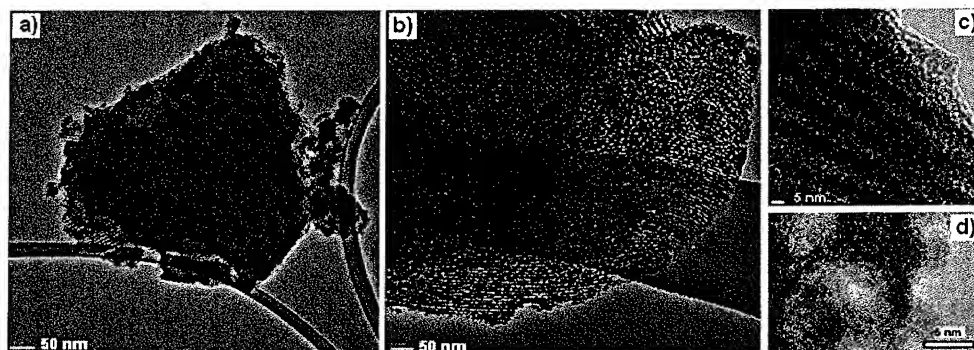
Figure 3. TEM images of (a) meso-13Cd(II)-60TiO$_2$ and (b–d) meso-13CdS-60TiO$_2$ at different magnifications.

(Figure 3). The TEM images were collected using the samples that are calcined at 250, 300, and 350 °C because the fresh samples and the samples treated at up to 130 °C are damaged under the electron beam in the TEM. The samples calcined at over 300 °C display crystalline walls. The spacing between the repeating features in the TEM images have a 7.3 nm spacing, corresponding (100) planes of the mesostructured samples (Figure 3). The observed distances in the images and the (100) diffraction line are consistent with each other. Figure 3a shows a TEM image of the film sample before the H$_2$S treatment, and all other images are obtained from the same sample after the H$_2$S reaction. It is difficult to collect HR-TEM images of the samples for better resolution because the samples are very sensitive to the electron beam. However, the images collected over 1.0 s clearly display the mesostructures and crystalline domains on the walls. The titania walls are amorphous at 250 °C. Note also that the wide-angle XRD patterns of relatively thicker film samples show only broad diffraction lines due to nanocrystalline CdS. Therefore, the crystalline parts of the walls must be CdS nanoparticles. Similar images were also obtained from the meso-CdSe-TiO$_2$ film samples.

It is important to note that the CdS and CdSe nanoparticles undergo decomposition upon reaction with nitric acid, both in the mesostructured silica[23] and titania. Notice that the H$_2$S or H$_2$Se and nitrate ion reaction produces excessive amounts of nitric acid in the media. There are two nitrate ion sources, namely, the nitric acid (used to stabilize titania species in the solution phase) and cadmium nitrate (used as a Cd(II) ion source) in the reaction mixture. Therefore, the nitrate ions, which are important during the assembly of mesostructured films, need to be removed from the media before or right after the H$_2$S (or H$_2$Se) reaction. We have solved this problem in the case of silica by washing the product after H$_2$S treatment.[17] This process safely removes the nitric acid formed upon the H$_2$S reaction. However, in the case of titania films, washing causes other complications on the titania framework (the film samples lose their transparency and usually get washed out of the substrate), and the coordinated nitrate ions cannot be completely removed from the titania matrix by washing. Therefore, washing may not be a good solution to stabilizing the CdS and CdSe nanoparticles in the titania channels.

The nitrate ion, upon spin or dip coating, remains in the film samples and interacts with the metal centers through coordination as monodentate, bidentate, and/or bridged ligands. The asymmetric stretching mode of the nitrate ion, which is doubly degenerate in the free ion, splits into two peaks in the 1290–1600 cm^{-1} region. Figure 4 shows FTIR spectra of three samples, which were prepared using HCl (as the acid source, labeled as meso-TiO$_2$) and HNO$_3$ with a Cd(II)/P123 mol ratio of 2 and
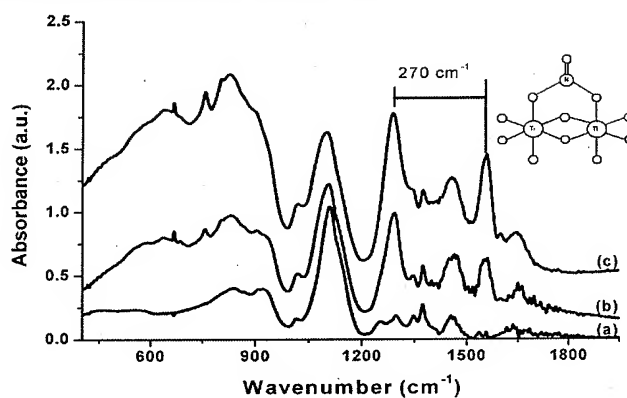

Figure 4. FTIR spectra of (a) mesostructured titania prepared using HCl as the acid source with a Ti/P123 mol ratio of 60 and samples prepared using HNO$_3$ with a Cd/P123 mol ratio of 2 and Ti/P123 mol ratios of (b) 40 and (c) 80.

Ti(IV)/P123 mol ratios of 40 and 80 (labeled as meso-2Cd(II)-40TiO$_2$ and meso-2Cd(II)-80TiO$_2$). Notice that the peaks at 1290, 1475, and 1560 cm^{-1} appear if the acid source is changed from hydrochloric acid to nitric acid with the addition of cadmium nitrate (cf. spectrum a with spectra b and c in Figure 4). The intensity of the peaks at 1290 and 1560 cm^{-1} further increases with an increasing Ti(IV)/P123 mol ratio from 40 to 80 (cf. spectra b and c in Figure 4). The peaks at 1290, 1475, and 1560 cm^{-1} originate from the asymmetric stretching mode of the coordinated nitrate ions. The peaks at 1290 and 1475 cm^{-1} collectively belong to the nitrate ions coordinated to the Cd(II) species, and the peaks at 1290 and 1560 cm^{-1} are due to nitrate ions coordinated to the Ti(IV) surface sides. The splitting energy, ca. 185 cm^{-1} in the Cd(II) sides and 270 cm^{-1} in the Ti(IV) surface sides, indicates that the nitrate ions are coordinated as a bidentate and bridged ligands to the Cd(II) and Ti(IV) sites, respectively.

The assignments were based on our further observations after changing the Cd(II) and Ti(IV) contents of the samples. The cadmium nitrate free samples display peaks only at 1290 and 1560 cm^{-1}; these are assigned to nitrate ions coordinated to Ti(IV) and the peak at 1475 cm^{-1} appears only in the presence of the cadmium nitrate in the media. Notice that the peaks at 1290 and 1560 cm^{-1} gradually increase with increasing titania content for a Ti(IV)/P123 mol ratio of 40–80 , clearly proving that these signals are the nitrates coordinated to the titania sides. The spectra in Figure 5 are from the samples with a Ti(IV)/P123 mol ratio of 60 with increasing Cd(II) in the samples (meso-xCd(II)-60TiO$_2$, where x is 2, 10, and 13). It is clear from the trend
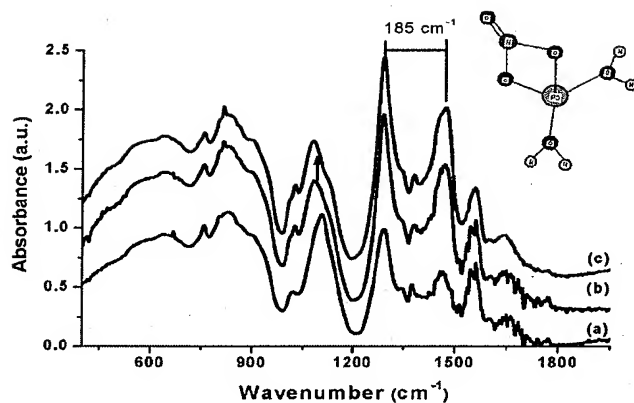
Figure 5. FTIR spectra of three fresh samples with a Ti/P123 mol ratio of 60 and Cd(II)/P123 mol ratios of (a) 2, (b) 10, and (c) 13. The inset shows the nitrate ion Cd(II) coordination.
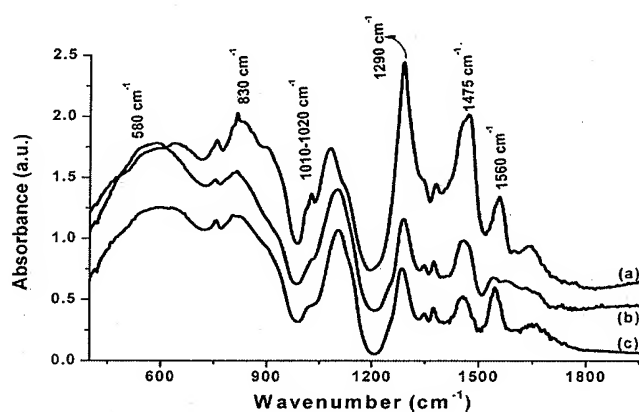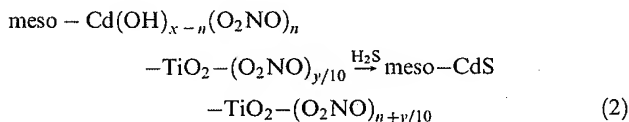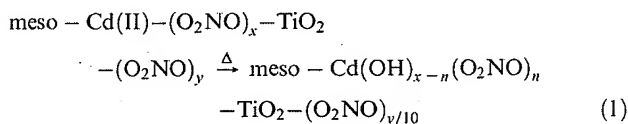

Figure 6. FTIR spectra of a sample with a Ti/P123 mol ratio of 60 and a Cd(II)/P123 mol ratio of 13 for (a) a fresh sample, (b) a sample aged at 130 °C for 4 h, and (c) a sample after H$_2$S treatment.

in the spectra that the intensity of the nitrate ions coordinated to Ti(IV) does not change; however, the peaks at 1290 and 1475 cm^{-1} gradually increase with increasing Cd(II) content of the samples, indicating that these two peaks belong to nitrate ions coordinated to Cd(II) sites. The schematic representation of those coordinative interactions of the nitrate ions with Cd(II) and titania is also shown in the insets in Figures 4 and 5. Note also that the nitrate ions undergo a ligand exchange with coordinated water molecules of the Cd(II) ions and display peaks at 1290 and 1475 cm^{-1} in the [Cd(H$_2$O)$_4$](NO$_3$)$_2$/P123 liquid-crystalline mesophases.[18] Therefore, there is no ambiguity in the above assignments, and they can be used to monitor the aging and H$_2$S (or H$_2$Se) reaction processes. Similarly, the titania surface and walls, under acidic conditions, consist of coordinated water molecules (protonated Ti—OH sites, Ti—OH$_2$) that also undergo ligand exchange with the nitrate ions.

Both sets of peaks, due to the Cd(II)-(O$_2$NO) and Ti-(IV)-(O$_2$NO) species, lose intensity upon aging the samples at 130 °C (Figure 6). A majority of the nitrate signals disappear upon heating the samples at 130 °C for 4 h without losing the mesostructured integrity of the film samples. The aging step was also repeated for the cadmium nitrate free samples in which the behavior of the nitrate signals is very similar, indicating that nitrate removal is carried out over the titania sides. If the aging is

carried out under high humidity, the removal of the nitrate ions is faster. However, it is difficult to remove all nitrate ions from the media. The remaining small number of nitrate ions coordinates to the titania surface sides upon H$_2$S (or H$_2$Se) reaction. Notice that the peak intensity at 1290 cm^{-1}, which is common for both nitrates, remains unaltered but the peak at 1475 cm^{-1}, due to the Cd-O$_2$NO sides, completely disappears and the peak at 1540 cm^{-1} due to nitrates on the titania sides is almost completely recovered upon H$_2$S reaction (Figure 6). These observations indicate that the nitrate ions coordinated to the Cd(II) are replaced by Cd—S bonds and the liberated nitrate ions coordinate to the titania surface. Possible reaction mechanisms during aging and the H$_2$S reaction are shown in eqs 1 and 2, where x depends on the Cd(II) incorporated, n is $^x/_{10}$, and y is the number of nitrate ions on the surface of the titania that is also reduced by a factor of 10 during the aging step. The value of y is around 3 to 4, which also doubles by increasing the titania content from a mol ratio of 40 to 80 if we assume that the absorption extinction coefficients of the nitrate ion coordinated to the Cd(II) and Ti(IV) sides are the same (Figure 4). The small shift from 1560 to 1540 cm^{-1} may originate from the change in the environment of the nitrate ions coordinated to the titania sides that are further condensed during the aging step. A similar mechanism is valid in the H$_2$Se reaction step, but the H$_2$Se reaction is more problematic (discussed later).

$$\text{meso} - \text{Cd(II)}-(\text{O}_2\text{NO})_x-\text{TiO}_2$$
$$-(\text{O}_2\text{NO})_y \xrightarrow{\Delta} \text{meso} - \text{Cd(OH)}_{x-n}(\text{O}_2\text{NO})_n$$
$$-\text{TiO}_2-(\text{O}_2\text{NO})_{y/10} \tag{1}$$

$$\text{meso} - \text{Cd(OH)}_{x-n}(\text{O}_2\text{NO})_n$$
$$-\text{TiO}_2-(\text{O}_2\text{NO})_{y/10} \xrightarrow{\text{H}_2\text{S}} \text{meso}-\text{CdS}$$
$$-\text{TiO}_2-(\text{O}_2\text{NO})_{n+y/10} \tag{2}$$

The condensation of the titania species is obvious from the changes in the broad peaks at around 580 cm^{-1} (gradually increases) and 830 cm^{-1} (gradually decreases, which is due to the δ-TiOH deformation mode) upon aging. Notice also that aging influences the interaction of the surfactant molecules with the metal ion species. The peak at 1080 cm^{-1} due to v-CO of the ethylene oxides shifts to 1105 cm^{-1} upon aging and H$_2$S (or H$_2$Se) reactions. The original shift of this peak from 1105 cm^{-1} (for pure P123) to 1080 cm^{-1} (after mixing with cadmium nitrate salt) is due to the hydrogen bonding interaction of the ethylene oxide and coordinated water (Cd-OH$_2$) that seems to be completely removed by aging at 130 °C (most likely due to formation of cadmium-oxy-hydroxy species) and H$_2$S or H$_2$Se treatment (due to the formation of CdS or CdSe nanoparticles).

The H$_2$S reaction with meso-Cd(II)-TiO$_2$ films produces CdS nanoparticles independently of the amount of H$_2$S and the duration of H$_2$S exposure, but the H$_2$Se reaction produces an extensive number of Se species if the H$_2$Se concentration is high (greater than 120 Torr) and if the samples are kept under H$_2$Se far too long. The Raman spectra of the samples that are kept at over 100 Torr of H$_2$S display a peak at 252 cm^{-1} due to the polymeric Se chain.[27] The EDS data also show a higher Se/Cd ratio, between 2 and 30, compared to the bulk ratio, 1.28 in the CdSe. Figure 7a shows an SEM image with selected area EDS data of a sample

(27) Li, I. L.; Zhai, J. P.; Launois, P.; Ruan, S. C.; Tang, Z. K. *J. Am. Chem. Soc.* **2005**, *127*, 16111.
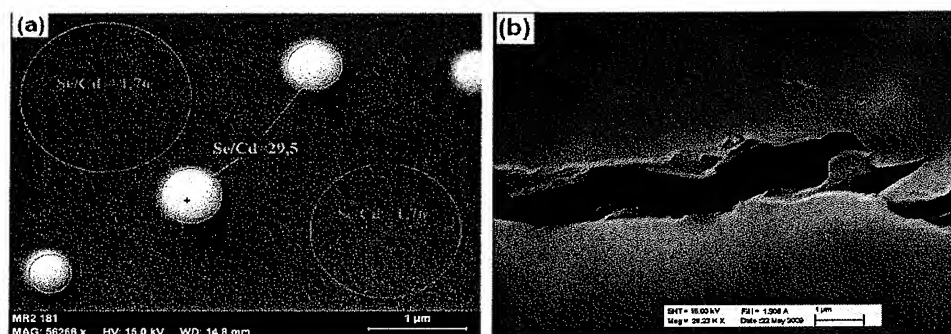
Figure 7. SEM images of the meso-13Cd(II)-60TiO$_2$ film samples after H$_2$Se reaction (a) under pure H$_2$Se and (b) under an H$_2$Se/N$_2$ atmosphere.

that contains a large amount of Se. The bright spherical particles originate from the Se particles. EDS and Raman spectroscopy must be used together to resolve this issue. Relying on just EDS and Raman can lead one to a wrong conclusion. We have observed exactly the same Se/Cd intensity of bulk in some samples, but they contained Se, which can be detected by Raman spectroscopy. In other samples, the Raman spectra displayed only CdSe peaks, but EDS showed us that the reaction was only 10% complete, where the Se/Cd intensity ratio was 0.13. Therefore, the amount of H$_2$Se, reaction time, and reaction conditions needed to be optimized to ensure clean CdSe nanoparticles in the mesostructured titania films using both EDS and Raman spectroscopy techniques. From a series of experiments under different conditions, we found that Se chain formation is a secondary process and is slower than CdSe formation. Se formation can be eliminated by carrying out the H$_2$Se reactions at lower H$_2$Se concentrations for shorter times, such as below 50 Torr of H$_2$Se for 1 min. However, this treatment (a diffusion-limited process) converts only 5 to 10% of the Cd(II) ions into CdSe nanoparticles. The diffusion of H$_2$Se into the films can be increased by exposing the samples to an H$_2$Se/air (close to atmospheric pressure of 50 Torr of H$_2$Se in 650 Torr of air) mixture. However, this also produces Se particles at higher H$_2$Se concentrations (higher than 50 Torr of H$_2$Se) and a small number of CdSe nanoparticles (10%) at lower H$_2$Se concentrations. CdSe formation can be enhanced by repetitive exposure of the samples to fresh H$_2$Se/air mixtures, but this is a costly process and after five repetitive exposures 50% CdSe formation can be achieved. Notice that Se formation is an oxidation process in which the Se^{2-} ion is oxidized to Se(0).[28] Therefore, the H$_2$Se reaction has to be carried out under a nonoxidizing environment to obtain stable meso-*x*CdSe-*y*TiO$_2$ films. We have carried out the H$_2$Se reaction under an N$_2$ atmosphere, which ensures the complete conversion of Cd(II) ions to CdSe nanoparticles in one step with no Se formation detected. The SEM images in Figure 7 clearly show that the samples under pure H$_2$Se produce a large number of segregated Se particles with a homogeneous small number of CdSe nanoparticles embedded into the pores, but the reaction under H$_2$Se/N$_2$ converts all of the Cd(II) into CdSe nanoparticles. The thicker samples crack upon H$_2$Se reaction as a result of a complete H$_2$Se reaction. These samples are quite light-sensitive and undergo slow decomposition to Se under a green laser. The details of these studies will be published elsewhere.

The clean, stable samples were further analyzed using EDS and Raman techniques. Figure 8 displays the EDS data of bulk CdS
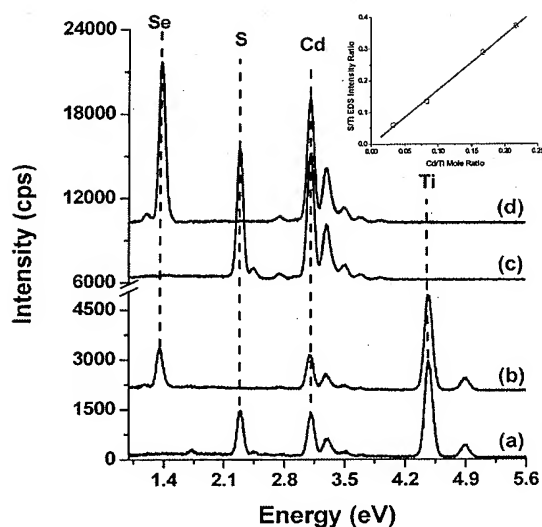
(28) Tang, Z.; Wang, Y.; Sun, K.; Kotov, N. A. *Adv. Mater.* **2005**, *17*, 358.

Figure 8. EDS data of (a) meso-13CdS-60TiO$_2$, (b) meso-10CdSe-60TiO$_2$, (c) bulk CdS, and (d) bulk CdSe. The inset is a plot of the intensity ratio of S/Ti, measured using EDS, versus the Cd/Ti mole ratio, incorporated into the film samples, of meso-*x*CdS-60TiO$_2$ (where *x* is 2, 5, 10, and 13).

and CdSe and meso-13CdS-60TiO$_2$ and meso-10CdSe-60TiO$_2$. The S/Cd and Se/Cd intensity ratios of the samples and bulk crystalline samples are the same, indicating that the samples are pure CdS and CdSe, respectively, and that all of the Cd(II) ions are converted into CdS or CdSe without any other sulfur or selenium species in the film samples. The EDS data, which gives the intensity ratio of S/Ti versus the amount of Cd(II) incorporated, displays a linear correlation between the Cd(II) concentration incorporated during the synthesis step and the CdS in the film samples (inset in Figure 8). The Cd/S/Ti and Cd/Se/Ti intensity ratios are all consistent with the initial concentrations of Cd(II) and Ti(IV) in all samples after the H$_2$S and H$_2$Se reactions, respectively. The Raman spectra of the meso-CdS-TiO$_2$ samples display a weak peak at around 290 cm^{-1}, characteristic (longitudinal optical mode) of the CdS nanoparticles.[29] Similarly, the Raman spectra of the meso-CdSe-TiO$_2$ samples display up to three peaks at 207, 412, and 618 cm^{-1} due to the longitudinal optical mode[30] (LO) and the overtones (2LO and 3LO) of the

(29) Zeiri, L.; Patla, I.; Acharya, S.; Golan, Y.; Efrima, S. *J. Phys. Chem. C* **2007**, *111*, 11843.
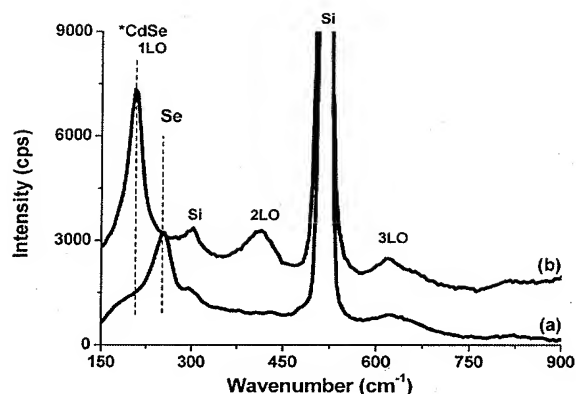(30) Tanaka, A.; Onari, S.; Arai, T. *Phys. Rev. B* **1992**, *45*, 6587.

Figure 9. Raman spectra of meso-13Cd(II)-60TiO$_2$ after the H$_2$Se reaction (a) under pure H$_2$Se and (b) under an H$_2$Se/N$_2$ atmosphere.

Figure 10. UV−vis absorption spectra of (a) fresh and (b) aged meso-13Cd(II)-60TiO$_2$ at 130 °C and (c) reacted with H$_2$S, (d) meso-13CdS-60TiO$_2$, and (e) meso-13CdSe-TiO$_2$ film samples. The spectra in (d) and (e) are recorded using thicker film samples.

CdSe nanocrystallites, respectively (Figure 9). The LO frequency is shifted from its bulk value, indicating that the observed peak at 207 cm^{-1} is due to CdSe nanocrystallites.[30] All other peaks in the spectra in Figure 9 are due to Si (substrate) or the surfactant.

The behavior of the nitrate ions can also be monitored using a UV absorption band at around 204 nm. The absorption band at 204 nm is due to the nitrate ions, and the broad shoulder at around 250 nm, which tails down to 330 nm is due to the titania in the UV region of the electromagnetic spectrum of the thin film samples (Figure 10). During aging, the band at 204 nm loses intensity, the temperature-dependent measurements display an isosbestic point at 230 nm, and the titania band slightly red shifts, collectively indicating the single-step decomposition of the nitrate ion from the media and the further condensation of the titania species, respectively. These observations are also consistent with the FTIR (the increase in the intensity of the peak at 580 cm^{-1} and the decrease in the δ-TiOH peak at 830 cm^{-1}) and XRD (shift of the diffraction lines to higher angles) results.

The UV−visible absorption spectra have also been recorded after H$_2$S and H$_2$Se treatments to determine the optical behavior and the particle sizes of the CdS and CdSe nanoparticles, respectively. Figure 10 displays extra absorption over 330 nm (the absorption edge tails down to 480 nm in the meso-CdS-TiO$_2$ and down to 530 nm in the meso-CdSe-TiO$_2$ samples) due to CdS or CdSe nanoparticles, respectively. The direct gap fitting of these bands gives band gap energies of 2.60 eV for the CdS particles and 2.36 eV for the CdSe particles. The band gap values correspond to 4.3 and 3.7 nm particles of CdS and CdSe, respectively. The particle sizes were determined using Darma and Sharma's tight binding model[31] and the derived empirical formula, where the shift in the band gap energy is given as $\Delta E_g = a_1 e^{-d/b1} + a_2 e^{-d/b2}$ (d is the diameter and the parameters a_1, b_1, a_2, and b_2 are 2.83, 8.22, 1.96, and 18.07 and 7.62, 6.63, 2.07, and 28.88 for the CdS and CdSe nanocrystallites, respectively).[31] Note also that size of the particle depends on the pore size and the nature of the pore walls. The fresh samples and the samples with a lower Ti(IV)/ P123 mol ratio have softer pore walls and larger unit cells (extra space between the walls) such that the CdS or CdSe produced in
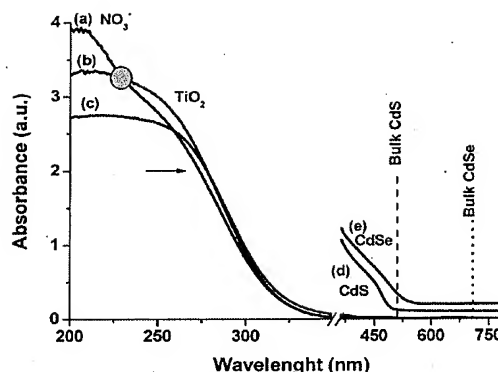
the freshly prepared film samples is slightly larger and the absorption edges display a red shift compared to their aged counterparts. This can be used to fine tune the band gap and the particle size of the CdS and CdSe nanocrystallites in the pore walls and pore surface. However, the nanoparticles synthesized using fresh samples are not stable. Therefore, this needs further study using pluronics such as F127 and the method developed in this work. The CdSe nanoparticles are light-sensitive and undergo CdSe to Se conversion upon exposure to the green laser of the Raman spectrometer.

Conclusions

Well-ordered, transparent mesostructured titania films can be prepared in the presence of cadmium nitrate and nitric acid over a broad range of Cd(II) and Ti(IV) concentrations. The film samples, aged first in a 50% humidity oven at RT and then at 130 °C in a regular oven, can be exposed to an H$_2$S or H$_2$Se/N$_2$ mixture to produce stable CdS or CdSe nanoparticles in the walls and channel spaces of mesostructured titania films, respectively. To ensure the stability of the nanoparticles in the mesostructured titania, the nitrate ions (which act as the acid source upon H$_2$S or H$_2$Se reaction) need to be removed from the media. The coordination of the nitrate ion to the titania and Cd(II) species promotes the thermal decomposition of the nitrate ions from the media with a gentle aging step. The pure H$_2$S reaction produces CdS nanoparticles, but the H$_2$Se reaction must be carried out under an N$_2$ atmosphere to eliminate secondary reactions, such as the formation of Se species. The stabilized CdS and CdSe nanoparticles are crystalline with average particle sizes of 4.3 and 3.7 nm with optical band gaps of 2.60 and 2.36 eV, respectively. However, the particle size can be changed by changing the pore size and wall softness of the titania films. The behavior of the particle size with respect to the softness of the host media and the light sensitivity of CdSe nanoparticles needs further study. These materials are good candidates for solar energy applications.

(31) Sapra, S.; Sarma, D. D. *Phys. Rev. B* **2004**, *69*, 125304.

Synthesis of mesoporous TiO$_2$ with a crystalline framework

Yinghong Yue and Zi Gao*

Department of Chemistry, Fudan University, Shanghai 200433, P.R. China. E-mail: zigao@fudan.edu.cn

A thermally stable mesoporous TiO$_2$ with a crystalline framework and ordered large pores is synthesized using a block copolymer as a structure-directing agent through an N^{0}I^0 assembly pathway, followed by a hydrothermal process.

The synthesis of mesoporous silica with a high surface area and uniform cylindrical mesopores, which was designated as M41S, was first demonstrated in 1992.[1] Since then, the use of surfactants and amphiphilic block copolymers to organize mesoporous structures has been extended to the preparation of non-silica mesoporous metal oxides. Mesoporous MnO$_2$,[2] Al$_2$O$_3$,[3,4] TiO$_2$,[4,5] Nb$_2$O$_5$,[4,6] Ta$_2$O$_5$,[4,6] ZrO$_2$[4,7] and SnO$_2$[4,8] have been synthezied over the past few years. Among them, mesoporous TiO$_2$ is most attractive due to its excellent performance in photocatalytic reactions.[9] It is well known that the effectiveness of titania as a photocatalyst is very sensitive to its crystal phase, particle size and crystallinity, and the mesoporous TiO$_2$ prepared using phosphate surfactants has low photocatalytic activity because the amorphous titania channel walls afford low quantum yield for photocatalytic reactions.[10] Calcination of the as-synthesized mesoporous TiO$_2$ at high temperature is essential for the crystallization of titania in the channel wall.[4] However, damage to the integrity of the mesoporous structure will take place upon calcination at high temperature, thus only mesoporous TiO$_2$ with amorphous or semicrystallized channel walls have been reported till now. Here we present the first example of mesoporous TiO$_2$ with crystalline framework, prepared through an N^{0}I^0 assembly pathway using a triblock copolymer as a structure-directing agent and followed by a hydrothermal process.

The mesoporous titania with crystalline framework was prepared as follows: a calculated amount of titanium ethoxide Ti(OC$_2$H$_5$)$_4$ was dissolved in an ethanol solution containing triblock poly(ethylene oxide)–poly(propylene oxide)–poly(ethylene oxide) (EO$_{20}$PO$_{70}$EO$_{20}$, Aldrich) and a very small amount of CeCl$_3$ which acts as a stabilizer in the syntheses.[11] After stirring for 1 h at ambient temperature, a water–ethanol mixture containing a 20% molar fraction of water was added dropwise. The molar composition of the reaction mixture was: 0.05 Ce^{3+} : 1.0 TEOT : 0.02 EO$_{20}$PO$_{70}$EO$_{20}$: 4.0 H$_2$O : 15.5 C$_2$H$_5$OH. The mixture was stirred at ambient temperature for another 48 h. In the hydrothermal process, a large amount of water was added to the resulting solution until the H$_2$O/TiO$_2$ molar ratio = 90. Then, the mother liquor containing the precipitate was transferred to a stainless steel autoclave, and heated at 80–180 °C for 24 h. The product obtained was filtered off, washed with distilled water, dried at 100 °C, and finally calcined in air at 350 °C or 500 °C for 4 h. The samples studied are denoted as TiO$_2$-x-y, where x and y represent the temperatures of hydrothermal aging and calcination, respectively. A mesoporous TiO$_2$ sample untreated hydrothermally was also prepared for comparison.

Fig. 1 shows the results of wide-angle X-ray diffraction studies performed on a Rigaku D/MAX-IIA diffractometer using Cu-Kα radiation of the hydrothermally treated mesoporous titania before and after calcination. No clear diffraction peaks are observed for as-synthesized mesoporous TiO$_2$ without hydrothermal treatment before calcination. After calcination weak and broad peaks, which can be indexed as the

(101), (004), (200), (105) and (204) reflections of anatase crystalline phase, appear on the pattern, showing that the channel walls are semicrystallized and some anatase nanocrystallites are formed and embedded in the amorphous titania channel walls. In contrast, sharp diffraction peaks of anatase appear on the XRD patterns of samples hydrothermally treated at 80–180 °C even before calcination and the intensity of the peaks increases little after calcination, indicating that the channel walls of the mesoporous oxides can be successfully crystallized at the low hydrothermal treatment temperatures. The crystals in the TiO$_2$-120-350 and TiO$_2$-180-350 samples are estimated to be of size 10 and 15 nm, respectively, by applying the Scherrer formula on the (101) diffraction peaks. The degree of crystallization and the anatase crystal size increase as the hydrothermal treatment temperature is increased from 80 to 180 °C. A brookite peak at 31° (2θ) appears for samples treated at 180 °C. Calcination up to 500 °C does not have significant effects on the diffraction patterns of the samples, showing that the anatase crystal phase is retained at this temperature and no phase transformation has occurred.

Thermogravimetric experiments of the hydrothermally treated samples carried out in flowing air on a Rigaku Thermoflex instrument indicate that there are three endothermic processes in the TG/DTG/DTA curves at 20–120 °C, 120–320 °C and 320–420°C, corresponding to the release of adsorbed water, block copolymer and structural water, respectively. Therefore, the block copolymer template in this type of mesoporous TiO$_2$ samples can be completely removed upon calcination in air at 350 °C.

Transmission electron micrographs of the TiO$_2$-120-350 sample recorded on a Philips CM 200 FEG Microscope (Fig. 2) shows that the pore channel walls are not totally continuous and the mesostructure is spotted with a few micro-domains of less ordered worm-like pore symmetry. Selected-area electron diffraction patterns (Fig. 2 inset) recorded on the same sample
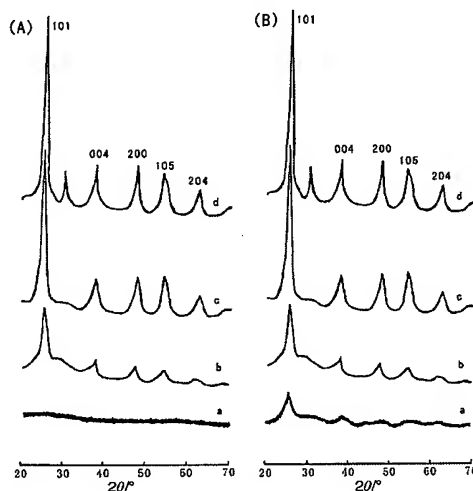

Fig. 1 XRD patterns of mesoporous TiO$_2$ before (A) and after (B) calcination. (a) TiO$_2$; (b) TiO$_2$-80-350; (c) TiO$_2$-120-350; (d) TiO$_2$-180-350.
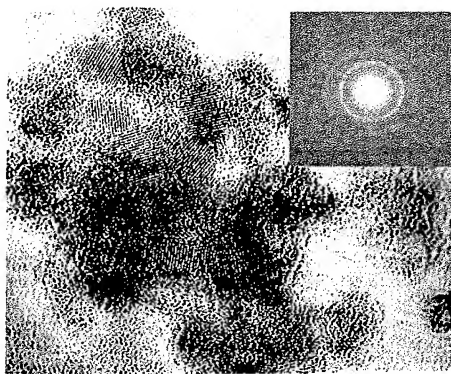
Fig. 2 TEM image and selected-area electron diffraction pattern (inset) of the TiO$_2$-120-350 sample

confirm that the channel walls are comprised of nanocrystalline anatase displaying characteristic diffuse electron diffraction rings.

Fig. 3 illustrates the N$_2$ adsorption/desorption isotherms of the TiO$_2$-120-350 sample measured using a Micromeritics ASAP 2000 system. A large H1-type hysteresis loop at high relative pressure is observed, which is related to the capillary condensation associated with large pore channels. BJH analysis of the desorption isotherm is shown in Fig. 3 (inset). The narrow gaussian pore size distribution curve implies that the material has very regular pore channels in the mesoporous region. The textural properties of all the hydrothermally treated samples are listed in Table 1 along with the data of the untreated samples. The pore size and volume of the hydrothermally treated samples are significantly greater than those of the untreated sample, whereas their specific surface areas are slightly lowered. The dramatic increase in pore size of the samples shows that the mesoporous TiO$_2$ could be restructured under hydrothermal treatment in the presence of the block copolymer template. The
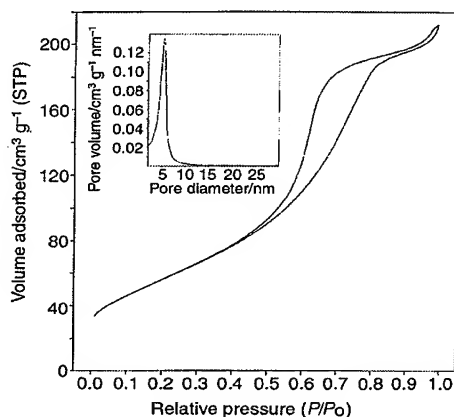
Table 1 Textural properties of mesoporous TiO$_2$ samples

Sample	Aging temperature/ °C	Calcination temperature/ °C	BET surface area/m^2 g^{-1}	Pore diameter/ nm	Pore volume/ cm^3 g^{-1}
TiO$_2$-80-350	80	350	201	4.4	0.271
TiO$_2$-80-500	80	500	150	5.2	0.249
TiO$_2$-120-350	120	350	204	5.5	0.315
TiO$_2$-120-500	120	500	157	6.2	0.302
TiO$_2$-180-350	180	350	159	7.0	0.366
TiO$_2$-180-500	180	500	134	8.0	0.336
TiO$_2$	none	350	242	2.2	0.156
TiO$_2$	none	500	191	2.0	0.130

pore sizes of TiO$_2$-180-350 and TiO$_2$-180-500 reach 7.0 and 8.0 nm, respectively, which are the largest reported for mesoporous titania until now.[4] The mesoporous TiO$_2$ materials with crystalline framework retain their structural integrity and mesoporosity when calcined at 500 °C.

This work shows that mesoporous TiO$_2$ materials with anatase crystalline framework can be successfully prepared using a templating procedure followed by hydrothermal treatment and calcination. Amorphous titania in the channel walls of the mesoporous structure is crystallized at low hydrothermal temperature without sacrificing porosity and pore regularity, and the template is removed at a relatively low calcination temperature to ensure the materials against structure degradation. The crystalline framework, high specific surface area, large pore size and high thermal stability of these new materials are expected to afford better activity toward photocatalytic reactions, in particular those concerned with bulky molecules and high space velocity.

Notes and references

1 C. T. Kresge, M. E. Leonowicz, W. J. Roth, J. C. Vartuli and J. S. Breck, *Nature*, 1992, **359**, 710.
2 Z. Tian, W. Tong, J. Wang, N. Duan, V. V. Krishnan and S. L. Suib, *Science*, 1997, **276**, 926.
3 S. A. Bagshaw and T. J. Pinnavaia, *Angew. Chem., Int. Ed. Engl.*, 1996, **35**, 1102.
4 P. Yang, D. Zhao, D. I. Margolese, B. F. Chmelka and D. G. Stucky, *Chem. Mater.*, 1999, **11**, 2813.
5 D. M. Antonelli and J. Y. Ying, *Angew. Chem., Int. Ed. Engl.*, 1995, **34**, 2014.
6 D. M. Antonelli and J. Y. Ying, *Chem. Mater.*, 1996, **8**, 874.
7 J. A. Knowles and M. J. Hudson, *J. Chem. Soc., Chem. Commun.*, 1995, 2083.
8 K. G. Severin, T. M. AbdelFattah and T. J. Pinnavaia, *Chem. Commun.*, 1998, 1471
9 Z. B. Zhang, C. C. Wang, R. Zakaria and J. Y. Ying, *J. Phys. Chem. B*, 1998, **102**, 10871.
10 V. F. Stone and R. J. Davis, *Chem. Mater.*, 1998, **10**, 1468.
11 W. Zhang and T. J. Pinnavaia, *Chem. Commun.*, 1998, 1185.

Fig. 3 N$_2$ adsorption/desorption isotherm and BJH pore size distribution plot (inset) of the TiO$_2$-120-350 sample at 77 K.